



ORIGINAL ARTICLE

Boosted performance of NiOx/Pt nanocatalyst for the electro-oxidation of formic acid: A substrate's functionalization with multi-walled carbon nanotubes



Islam M. Al-Akraa^{a,*,1}, Ahmed E. Salama^a, Yaser M. Asal^a,
Ahmad M. Mohammad^b

^a Department of Chemical Engineering, Faculty of Engineering, The British University in Egypt, Cairo 11837, Egypt

^b Chemistry Department, Faculty of Science, Cairo University, Cairo 12613, Egypt

Received 3 July 2021; accepted 8 August 2021

Available online 16 August 2021

KEYWORDS

Formic acid;
Platinum;
Nickel oxide;
Carbon nanotubes;
Poisoning;
Fuel cells

Abstract A NiOx/Pt nanostructured catalyst was developed on a glassy carbon substrate that was functionalized with “mutli-walled” carbon nanotubes (CNTs) for the electro-oxidation of formic acid (EOFA); the essential oxidation reaction in the direct formic acid fuel cells (DFAFCs). The sequential deposition technique was adapted for the electrodeposition of platinum (n-Pt) and nickel oxide (n-NiOx) nanoparticles onto a CNTs-functionalized glassy carbon (GC) substrate. The presence of CNTs in the catalyst restricted the deposition of n-Pt and n-NiOx mostly onto their walls. Interestingly, this NiOx/Pt/CNTs/GC catalyst displayed a significant enhancement in the catalytic activity toward EOFA. This occurred by driving the reaction mechanism exclusively via the desirable direct dehydrogenation pathway with a large (−116 mV) shift (relative to that of the Pt/GC catalyst) in the onset potential with a complete suppression for the undesirable poisoning dehydration route. It also offered a much (up to 5-fold) better tolerance against the CO poisoning that normally deteriorates the performance of the DFAFCs. The electrochemical impedance spectroscopy and the Tafel representations agreed on the effective role of n-NiOx in improving the electronic properties of Pt at the surface. On parallel, an oxidative stripping voltammetry of CO from

¹ The British University in Egypt (BUE), El Sherouk City, Cairo, Suez Desert Road Postal No. 11837, Egypt.

* Corresponding author.

E-mail address: islam.ahmed@bue.edu.eg (I.M. Al-Akraa).

Peer review under responsibility of King Saud University.



the NiOx/Pt/CNTs/GC catalyst confirmed the potential geometrical influence of CNTs in the divergence of n-Pt that mitigated the CO poisoning.

© 2021 The Author(s). Published by Elsevier B.V. on behalf of King Saud University. This is an open access article under the CC BY-NC-ND license (<http://creativecommons.org/licenses/by-nc-nd/4.0/>).

1. Introduction

Energy is one of the most, if it was not the most, important and critical influential elements in our life, and before securing its continuous supply, life shall not proceed smoothly. The main concerns about the traditional energy sources (principally fossil fuels) that we rely, with a great extent, on are the non-renewability and its bad impacts to the environment. The situation gets more complicated when we have a shortage in fossil fuels and a huge population growth. This is a great catastrophe that pushed the scientific community to explore other reliable and green energy sources that guarantee a sufficient and clean power supply. One of these promising alternatives is the fuel cells (FCs) that excelled the lithium ion batteries in rural areas that normally lacks accesses to electrical power (Ong et al., 2017; Tanveer et al., 2021). They, moreover, outperformed rechargeable batteries in the energy density of the fuel that permitted longer operation times for electrical appliances (Ong et al., 2017). The refueling convenience and the long-lasting durability constituted additional merits for FCs over the lithium ion batteries that typically need hours to get charged and last only for several months (Grey and Hall, 2020). Recently, the liquid FCs (LFCs) that normally utilized alcohols (methanol, ethanol, propanol, ethylene glycol, glycerol) (Al-Akraa et al., 2019c; Armenta-González et al., 2016; Cruz-Reyes et al., 2020; El-Deab et al., 2015; Garg et al., 2016; Mari et al., 2020; Maya-Cornejo et al., 2016; Ong et al., 2017), acids (e.g., formic acid, FA) (Al-Akraa et al., 2015b), ethers (e.g., dimethyl ether) (Ong et al., 2017) and hydrazine (Asazawa et al., 2009) were suggested to replace the traditional H₂/O₂ FCs in their diverse stationary and portable applications. In fact, the risks associating the production, use, transportation and storage under high pressure of H₂ gas in addition to its low energy density have stimulated the replacement. On contrary, liquid fuels can be easily handled, are much safer than H₂ and own much higher energy densities. One of the simplest and most suitable liquid fuels is formic acid (FA, HCOOH) that has a low carbon content (a single carbon atom) which minimizes the environmental influence to climate change. It is also used in food industries which ensures its non-toxicity (Kim et al., 2019). Moreover, the electro-oxidation of formic acid (EOFA) is simple but endures a significant (1750 kW h L⁻¹) energy density (Ong et al., 2017). In the DFAFCs, FA features a negligible crossover via the Nafion membrane (the ionic conductive electrolyte) which saves the fuel and amplifies the output power. The DFAFCs have as well a large (1.40 V) theoretical open-circuit potential and energy efficiency (1.062 %) under standard conditions (25 °C, 1 atm) (Kiani et al., 2019).

Nevertheless, before moving into a real marketing for DFAFCs, several issues related to the catalyst (high loading,

expensive cost and poisoning), fuel (sluggish oxidation kinetics) and cell (durability) have to be resolved (Li et al., 2020). Effort has been started a few decades back and got enriched with the revolution of nanoscience where numerous nanocatalysts were developed (Al-Akraa et al., 2017; Al-Akraa et al., 2019d; Li et al., 2021; Xu et al., 2020a; 2020b). Platinum (the ideal catalyst for EOFA) was assembled in minute amounts (reducing the catalyst's cost) in the form of nanostructures of large surface area to volume ratios. Yet, the catalyst's poisoning that typically occurs with carbon monoxide (CO) that is released from the spontaneous dehydration of FA has still been unresolved.

Several strategies have been recommended to modify the "pristine" Pt surfaces with active/inactive metal(s)/metal oxide (s) to principally tune the electronic properties of Pt either to resist the adsorption of CO or to enhance its oxidation at low overpotentials (Li et al., 2020). Geometrically, this modification may tailor the active sites in a specific unfavorable orientation for CO poisoning. The literature is rich in resources for the hybrid bimetallic systems as the Pt-Au (Asal et al., 2019b), Pt-Pd (Al-Akraa et al., 2015a), Pt-Ru (Zhou et al., 2011), Pt-Rh (El Sawy and Pickup, 2019), Pt-Bi (Yoo and Rhee, 2016), Pt-Ni (Habibi and Delnavaz, 2011), trimetallic systems as the Au-Cu-Pt (Xie and Dimitrov, 2020), oxide-modified systems as the MnOx/Pt (Asal et al., 2019a), CuOx/Pt (El-Nagar et al., 2017), FeOx/Pt (Al-Qodami et al., 2018) and polymer modified systems as the polyaniline/Pt (Abd El-Moghny et al., 2017) that exhibited outstanding behavior for CO poisoning. The existence of minute amounts of possible inorganic and organic contaminations that perhaps enter the cell with water, air and/or in-situ generated as a result of the degradation of various parts of the FCs could fortunately contribute to the CO mitigation (El-Nagar et al., 2015). From another perspective, "mutli-walled" carbon nanotubes (CNTs) as one of the crucial conducting supporting materials can be used to enhance the electrical and structural properties of catalysts. They could be used to form a 3-dimensional (3D) structure on a membrane electrode assembly and to improve the mass transport of active species; resulting in a higher catalyst utilization ratio (Maturost et al., 2021). Several methods for the CNTs surface modification have also been developed (Maturost et al., 2021). Recently, we reported on the substrate-dependent activity of methanol oxidation where adding minute amount of CNTs could effectively improve the reaction kinetics and mitigate the inherent poisoning (Al-Akraa et al., 2019b). Herein, we report on the skillful amendment of Pt nanoparticles (n-Pt) with nanostructured nickel oxide (n-NiOx) on a CNTs-functionalized GC substrate that boosted the catalytic activity of EOFA and mitigated completely the CO poisoning. The exceptional activity of this nanocatalyst foresees the quick industrialization of DFAFCs in the near future.

2. Experimental

2.1. Catalyst fabrication

All chemicals employed in this investigation were of analytical grades and were used as received without any further purification. A cleaned glassy carbon (GC, $d = 3.0$ mm) electrode was served as a working electrode after regular cleaning procedure (Mohammad et al., 2018). An Ag/AgCl/NaCl (3 M) electrode and a spiral Pt wire were served as the reference and counter electrodes, respectively.

After cleaning, a charge of 10 mC ($5.05 \mu\text{g}$) was passed at the GC electrode to electrodeposit n-Pt potentiostatically at 0.1 V from 1 mM H_2PtCl_6 that was dissolved in 0.1 M Na_2SO_4 solution. This electrode will next be abbreviated as the Pt/GC electrode or catalyst. Then a further electrode's modification with n-NiOx was performed in two successive steps. The first was the electrodeposition (64 mC, $19.5 \mu\text{g}$) of metallic Ni at a constant potential of -1 V from an aqueous solution of 1 mM $\text{Ni}(\text{NO}_3)_2$ dissolved in 0.1 M acetate buffer solution (ABS, $\text{pH} = 4.0$). Next, the metallic Ni was passivated (oxidized) by cyclic voltammetry at 200 mV s^{-1} in 0.1 M phosphate buffer solution (PBS, $\text{pH} = 7$) between -0.5 and 1 V for 10 cycles. This electrode will be abbreviated as the NiOx/Pt/GC electrode.

For one catalyst, before the deposition of n-Pt and n-NiOx, the GC electrode was functionalized with CNTs (Multi-walled, internal diameter: $5\text{--}10$ nm, outer diameter: 25 nm, length: $10\text{--}30 \mu\text{m}$, specific surface area: $> 55 \text{ m}^2 \cdot \text{g}^{-1}$, purity: $> 99.9\%$). This was achieved by adding 10 mg of CNTs to 1 mL 5% Nafion/ethanol with a further sonication for 1 h. Then, $10 \mu\text{L}$ of the obtained suspension was spread evenly on the GC surface and left to dry in air at room temperature for 1 h. Finally, the CNT-modified GC electrode was washed with double distilled water. The CNT-modified GC electrode was subjected to further modifications with n-Pt and n-NiOx (as described previously) and the catalyst will next be abbreviated as the NiOx/Pt/CNTs/GC catalyst.

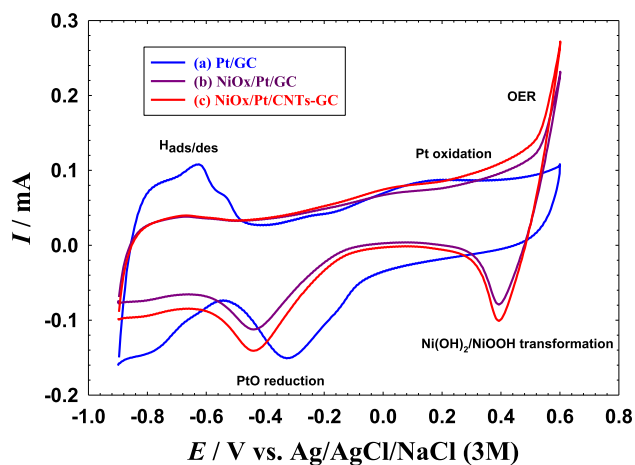


Fig. 1 CVs obtained at the (a) Pt/GC, (b) NiOx/Pt/GC and (c) NiOx/Pt/CNTs/GC electrodes in 0.1 M NaOH. Potential scan rate: 100 mV s^{-1} .

2.2. Electrochemical measurements

The electrochemical measurements were conducted at room temperature ($\sim 25 \pm 1$ °C) in a traditional three-electrode glass cell using a Bio-Logic SAS potentiostat (model SP-150) operated with EC-Lab software. The catalytic performance of the modified electrodes toward EOFa was investigated in 0.3 M FA solution ($\text{pH} = 3.5$).

2.3. Materials characterization

The morphology of the electrode was inspected using a field-emission scanning electron microscope (FE-SEM, QUANTA FEG 250) equipped with an energy dispersive X-ray spectrometer (EDS). The diffraction patterns of the modified electrodes were obtained by grazing incidence X-ray diffraction (XRD) spectroscopy operated with Cu $K\alpha$ ($\lambda = 1.54056 \text{ \AA}$) radiation at 45 kV and 360 mA (D8-DISCOVER, Bruker AXS). The inductively coupled plasma optical emission spectrometry, ICP-OES, (720 ICP-OES, Agilent Technologies) was utilized to assess the loss in the catalytic ingredients (Pt & Ni) after the electrochemical measurements.

3. Results and discussions

3.1. Electrochemical characterization

Fig. 1 shows the cyclic voltammograms (CVs) of the Pt/GC, NiOx/Pt/GC and NiOx/Pt/CNTs/GC electrodes that were measured at 100 mV s^{-1} in 0.5 M NaOH solution. The typical characteristic behavior of a poly-Pt electrode in an alkaline medium was obtained at the Pt/GC electrode (Fig. 1a), where the Pt \rightarrow PtO oxidation (-0.2 to 0.6 V), the PtO \rightarrow Pt reduction (at ca. -0.3 V), the hydrogen adsorption/desorption ($H_{\text{ads/des}}$, -0.5 to -0.9 V) peaks appeared in their regular potential domains (Al-Akraa and Mohammad, 2020; Asal et al., 2019a, b).

After the modification with n-NiOx (NiOx/Pt/GC electrode, Fig. 1b), the electrode kept its characteristic behavior of poly-Pt but with few informative changes;

- A decrease in the intensities of the $H_{\text{ads/des}}$ and PtO reduction peaks which agreed with the partial deposition of n-NiOx at the Pt surface (El-Nagar et al., 2013).
- A large increase in the anodic current after 0.4 V which denoted the catalytic effect of n-NiOx for the oxygen evolution reaction (OER) (Juodkazytė et al., 2019).
- A new redox couple appeared between 0.4 and 0.6 V which corresponded to the $\text{Ni}(\text{OH})_2/\text{NiOOH}$ transformation (Mohammad et al., 2015).
- A cathodic shift in the PtO reduction peak from -0.3 V to -0.4 V which was attributed to a possible change in the electronic properties of Pt at the electrode's surface due to the Pt-Ni interaction (Al-Akraa et al., 2019a).

Whereas, with the substrate's functionalization with CNTs (NiOx/Pt/CNTs/GC electrode, Fig. 1c), the previous features of the NiOx/Pt/GC electrode were conserved but with a little increase in the peak currents of $H_{\text{ads/des}}$, Pt oxidation and PtO reduction. A slight increase was also observed in the double layer capacitance that presumably originated from the high

Table 1 Electrochemical active surface areas and surface coverages of catalysts (data were taken from Fig. 1).

Electrode	ECSA, cm ²	θ , %
Pt/GC	0.44	–
NiOx/Pt/GC	0.25	43
NiOx/Pt/CNTs/GC	0.28	44 *

* Calculated based on the underlying Pt surface area for the Pt/CNTs/GC electrode (0.50 cm²)

specific surface area of the CNTs-modified electrode (Chen et al., 2002). Two important parameters could be calculated from Fig. 1; the electrochemical active surface area (ECSA) of the Pt (active component of the catalyst for EOFAs) and the surface coverage (θ) of n-NiOx (see Table 1). The ECSA of the three modified electrodes could be calculated using the following equation (Ong et al., 2015):

$$\text{ECSA}(\text{cm}^2) = \frac{Q_H(\mu\text{C})}{210\mu\text{Ccm}^{-2}} \quad (1)$$

where Q_H (μC) is the charge associated with the hydrogen desorption peaks (-0.5 to -0.9 V) and $210 \mu\text{C cm}^{-2}$ is the charge required to desorb a single monolayer of hydrogen from an ideal Pt surface (of 1 cm^2 cross-sectional) [29]. On the other hand, the surface coverage (θ) of n-NiOx was calculated using the following equation (Eq. (2)):

$$\theta\% = \left(1 - \frac{\text{ECSA}_{\text{modified}}}{\text{ECSA}_{\text{unmodified}}}\right) \times 100 \quad (2)$$

where $\text{ECSA}_{\text{modified}}$ is the surface area of the n-NiOx-modified electrode and the $\text{ECSA}_{\text{unmodified}}$ is the surface area of the unmodified electrode.

As mentioned previously, the decrease in ECSA of the NiOx/Pt/GC catalyst with the deposition of n-NiOx was normal as a portion of the Pt surface was covered with n-NiOx. The existence of CNTs as a substrate increased a little the ECSA of the NiOx/Pt/CNTs/GC electrode if compared to that of the NiOx/Pt/GC electrode; regardless their same n-Pt loading. This highlighted the important role of CNTs in the enhanced distribution of n-Pt which is desirable for EOFAs (Al-Akraa et al., 2019a).

3.2. Materials characterization

Morphologically, Fig. 2 shows the FE-SEM images of the Pt/GC, NiOx/Pt/GC and NiOx/Pt/CNTs/GC electrodes. Fig. 2A (Pt/GC electrode) shows the regular spherical nanoparticle shape of n-Pt (ca. 170 nm in diameter) with a large degree of aggregation. With the deposition of n-NiOx (Fig. 2B, NiOx/Pt/GC electrode) n-Pt could not be distinguished where they seemed encapsulated within the clusters of n-NiOx in large spheres of an average size of ca. 340 nm. On the other hand, in Fig. 2C (NiOx/Pt/CNTs/GC electrode), the CNTs are obviously seen intersected with their tubular structure (ca. 30 nm in diameter). Nevertheless, the exposed (uncovered with n-Pt) surface area of CNTs remained large. Also, as observed in Fig. 2B, n-Pt could not obviously be distinguished and seemed encapsulated within the clusters of n-NiOx that looked homogeneous, well-distributed, sometimes

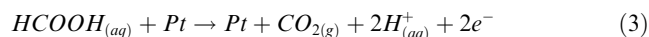
aggregated in cotton-like spherical particles of an average size of ca. 80 nm (Al-Akraa et al., 2019a). For the NiOx/Pt/CNTs/GC electrode, the deposition of n-NiOx was heavy to cover not only n-Pt but also CNTs. Interestingly, the presence of CNTs ensured the optimum divergence of n-Pt that hopefully will act against its surface poisoning. This morphological inspection came consistent with the surface area calculations (Table 1) in suggesting a large (43%) consumption of the n-Pt surface in the n-NiOx deposition.

The EDS analysis of the Pt/GC (Fig. 3a), NiOx/Pt/GC (Fig. 3b) and NiOx/Pt/CNTs/GC (Fig. 3c) electrodes confirmed the successful deposition of the different ingredients (C, O, Pt, Ni) and revealed their relative ratios in the catalyst (Table 2). Fig. 4 additionally provided the elemental mapping for the Pt/GC (Fig. 4A), NiOx/Pt/GC (Fig. 4B) and NiOx/Pt/CNTs/GC (Fig. 4C) electrodes which further confirmed the homogeneous distribution of n-NiOx and n-Pt at the surface of the underlying substrate.

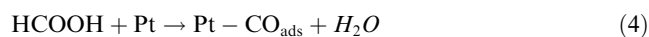
Furthermore, the XRD technique was utilized to investigate the crystal structure of the Pt/GC, NiOx/Pt/GC and NiOx/Pt/CNTs/GC electrodes, and their patterns are presented in Fig. 5. For all electrodes (Fig. 5a-c), several diffraction peaks were identified at ca. 25°, 43° and 79° corresponding, respectively, to the (002), (100) and (110) planes of the hexagonal carbon structure (JCPDS card No. 075-1621) (Keller et al., 2004). Also, the diffraction peaks identified at ca. 38°, 45°, 65° and 78° were assigned, respectively, to the (111), (200), (220), and (311) planes of the face-centered cubic (fcc) Pt lattice (JCPDS card No. 01-070-2057) (Huang et al., 2015). Exclusively at the n-NiOx-modified electrodes (Fig. 5b and c), the diffraction peaks at ca. 38°, 44° and 65° corresponded, respectively, to the (200), (111) and (220) planes of the nickel oxide (Cabañas Polo et al., 2012; Fazlali et al., 2015; Hailong et al., 2014; Li et al., 2017).

3.3. Catalysis of EOFAs

Fig. 6 shows the CVs of EOFAs at the Pt/GC, NiOx/Pt/GC and NiOx/Pt/CNTs/GC electrodes in an aqueous solution of 0.3 M formic acid (pH = 3.5). Indeed, EOFAs proceeded in two different routes (Kiani et al., 2019; Larsen et al., 2006; Lović et al., 2005). The first involved the dehydrogenation of FA to CO₂ (Eq. (3)). This direct route occurred at the Pt/GC electrode (Fig. 6A) at a low overpotential (~ 0.35 V) which certainly turns the actual voltage of DFAFCs close to the theoretical value. The peak current of this direct EOFAs was denoted as (i_p^d).



Alternatively, the dehydration of FA to CO was a parallel non-faradaic route (Eq. (4)) that could be launched at open circuit potentials. The produced CO was then adsorbed at the Pt surface; blocking a large portion of its active sites. That is why this route was undesirable for EOFAs.



With biasing the overpotentials highly in the anodic direction, the Pt surface became hydroxylated (Eq. (5)) which boosted the oxidative CO removal indirectly (Eq. (6)) at ca. 0.75 V with a peak current of (i_p^{ind}) that correlated to the CO poisoning level at the Pt surface.

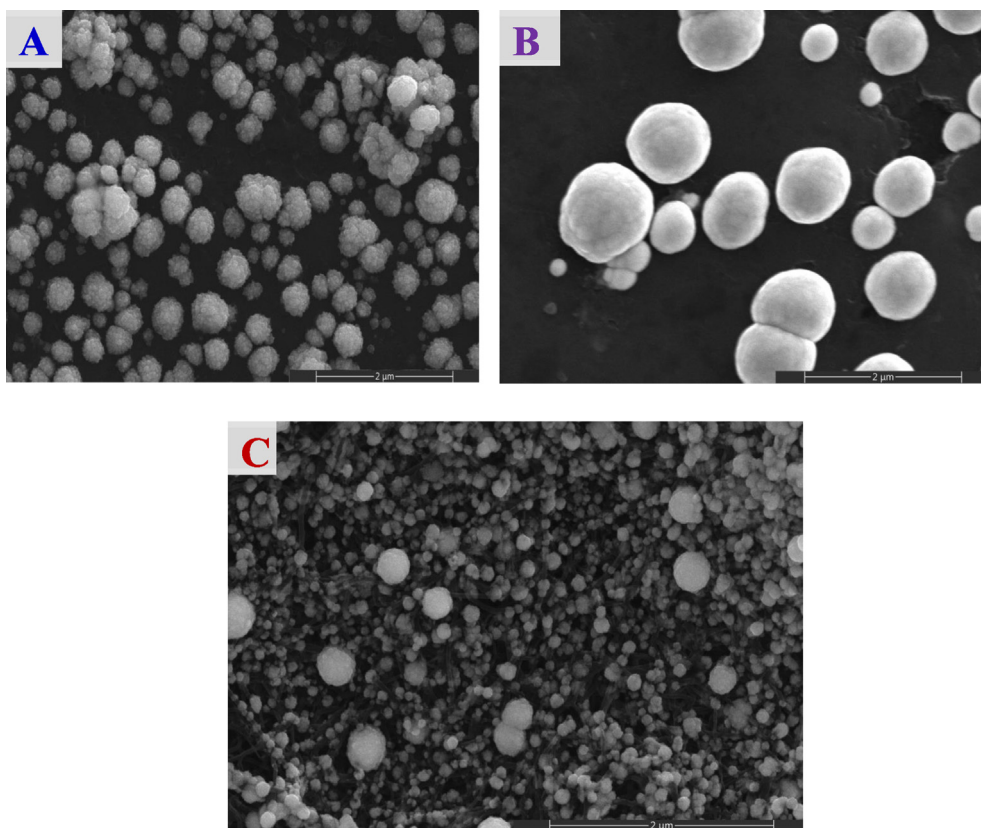


Fig. 2 FE-SEM images of the (A) Pt/GC, (B) NiOx/Pt/GC and (C) NiOx/Pt/CNTs/GC electrodes.

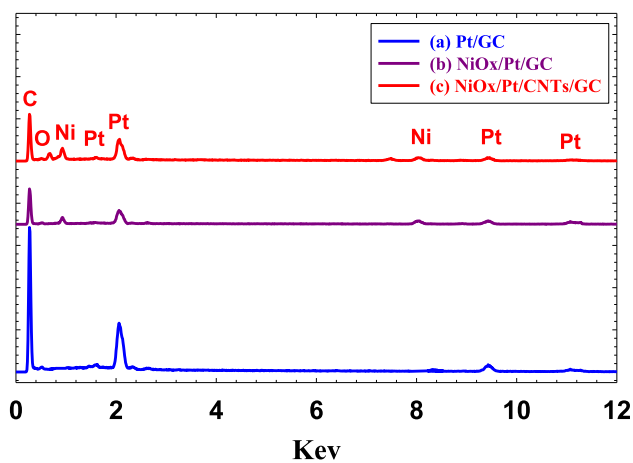
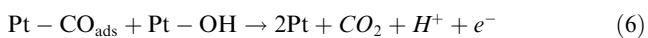
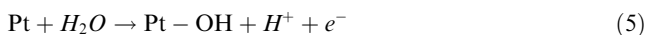


Fig. 3 EDS of the (a) Pt/GC, (b) NiOx/Pt/GC and (c) NiOx/Pt/CNTs/GC electrodes.



In the backward (cathodic-going) scan, after oxidizing most of the poisoning CO in the forward scan, EOFa could proceed mainly via the direct pathway (see the peak at ca. 0.4 V in the backward cathodic scan and its corresponding peak current, I_p^b).

The degree of catalytic enhancement toward EOFa and the inherent CO poisoning level were tracked by evaluating the

Table 2 A summary of the EDS data (Fig. 3).

Electrode	Element	Mass %
Pt/GC	C K	58.8
	O K	2.93
	Pt L	38.27
NiOx/Pt/GC	C K	69.15
	O K	7.18
	Ni K	0.57
NiOx/Pt/CNTs/GC	Pt L	23.1
	C K	57.84
	O K	2.85
	Ni K	5.22
	Pt L	34.36

ratios I_p^d/I_p^{ind} , I_p^d/I_p^b and the onset potential of EOFa (E_{onset}). A high I_p^d/I_p^{ind} ratio reflects a large number of free Pt active sites that can participate in the dehydrogenation route (Eq. (3)). While, a high I_p^d/I_p^b value reflects a low level of CO poisoning. Finally, the more negative E_{onset} is preferred to avoid the unnecessary high overpotentials. At the Pt/GC electrode (Fig. 6A), the values of I_p^d/I_p^{ind} , I_p^d/I_p^b and E_{onset} were ca. 0.69, 0.17 and -0.026 V. Although NiOx is inactive toward EOFa (Kiani et al., 2019; Mohammad et al., 2015), the catalytic activity of the NiOx/Pt/GC electrode (Fig. 6B) was higher than that of the Pt/GC electrode with I_p^d/I_p^{ind} , I_p^d/I_p^b and E_{onset} of 3.33 (i.e., 4.8 times higher), 0.40, and -0.028 V, respectively. This showed the improved catalytic performance of the NiOx/Pt/GC electrode toward EOFa. It has been reported that n-NiOx could accommodate the electrons involved in the EOFa

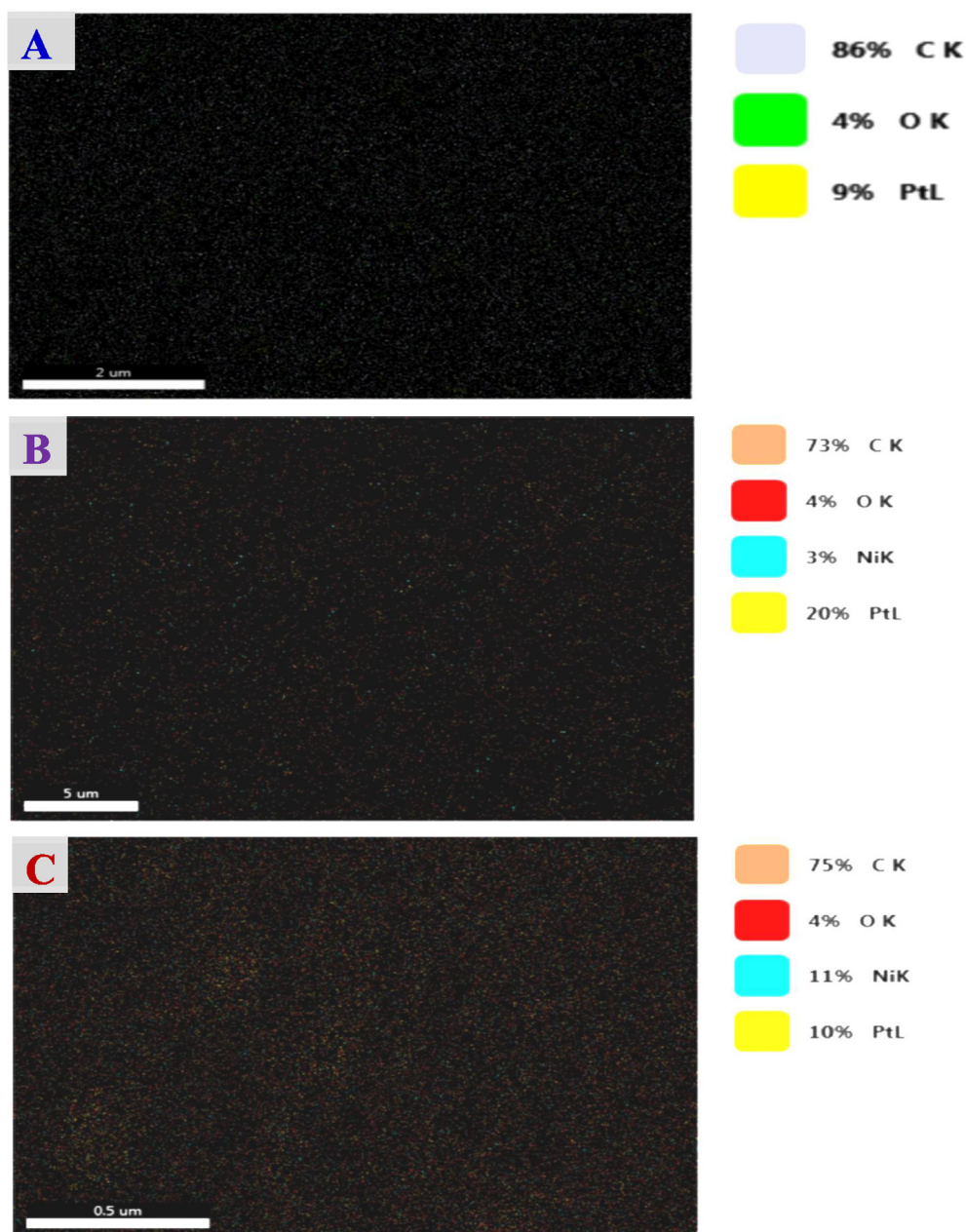


Fig. 4 Elemental mapping of the (A) Pt/GC, (B) NiOx/Pt/GC and (C) NiOx/Pt/CNTs/GC electrodes.

in the vacant d-orbital of Ni to mediate the reaction mechanism in the way speeding the charge transfer (El-Nagar et al., 2013; Mohammad et al., 2015). It could moreover enrich the Pt surface with oxygen/hydroxyl groups to enhance the oxidation of poisoning CO at relatively low overpotentials (El-Nagar et al., 2013; Mohammad et al., 2015). Surprisingly, the substrate's functionalization with CNTs (which is also inactive for EOFa (Al-Akraa et al., 2018; Lu et al., 2012)) could successfully vanish the CO poisoning of the NiOx/Pt/CNTs/GC electrode (Fig. 6C) with a catalytic performance excelling those of the Pt/GC and the NiOx/Pt/GC electrodes. The I_p^d/I_p^{ind} , I_p^d/I_p^b and E_{onset} of the NiOx/Pt/CNTs/GC electrode were infinity, 0.93 (5.5 times higher compared to the Pt/GC electrode) and -0.142 V (116 mV negative shift), respectively. Table 3 provided a summary of the I_p^d/I_p^{ind} , I_p^d/I_p^b

and E_{onset} values obtained from Fig. 6. It is interesting to observe the complete disappearance of the CO oxidation in Fig. 6C which indicated the successful mitigation of Pt poisoning. The significant (116 mV) negative shift in E_{onset} of the direct EOFa at the NiOx/Pt/CNTs/GC electrode is as well a plus in terms of amplifying the cell voltage. Table 4 presents a comparison between the electrochemical performance, in terms of I_p^d/I_p^{ind} , of the electrodes included in this investigation and others reported in literature.

From another perspective, the catalyst's stability is essential for the commercialization of DFAFCs. Fig. 7 shows the chronoamperometric current transients ($i-t$) in a 0.3 M aqueous solution of FA (pH 3.5) at 0.2 V at the Pt/GC, NiOx/Pt/GC and NiOx/Pt/CNTs/GC electrodes. The fast decay of the current density with time observed at the Pt/GC electrode

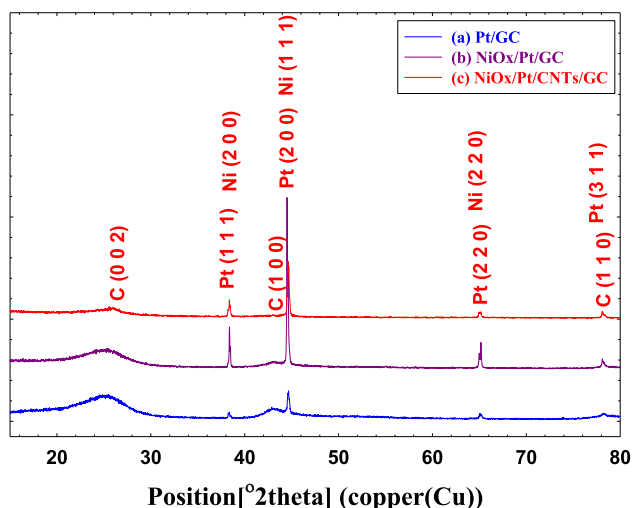


Fig. 5 XRD of the (a) Pt/GC, (b) NiOx/Pt/GC and (c) NiOx/Pt/CNTs/GC electrodes.

(Fig. 7a) reflected its poisoning during the EOFA (Shi et al., 2020; Yu et al., 2020). After the modification with n-NiOx (NiOx/Pt/GC electrode, Fig. 7b), the decay of current densities slowed down a little especially after 700 s. With the substrate's functionalization with CNTs (NiOx/Pt/CNTs/GC electrode, Fig. 7c), the current decay was the smallest and the catalyst owned the highest current density that reached ca. 0.4 mA cm^{-2} after 1800 s of continuous electrolysis (ca. 3 times higher than that obtained at Pt/GC and NiOx/Pt/GC electrodes).

Further, the inductively coupled plasma optical emission spectrometry (ICP-OES) was utilized to assess the loss in the catalytic ingredients (Pt & Ni) after the electrochemical inspection. Interestingly, the loss of the active material (Pt) in the Pt/GC, NiOx/Pt/GC and NiOx/Pt/CNTs/GC electrodes was minor below the detection limit of the instrument. This reflected the good stability of n-Pt under the working conditions. However, a minor loss of Ni (0.56 and 0.66 mg/L) was measured, respectively, for the NiOx/Pt/GC and NiOx/Pt/CNTs/GC electrodes (see Table 5).

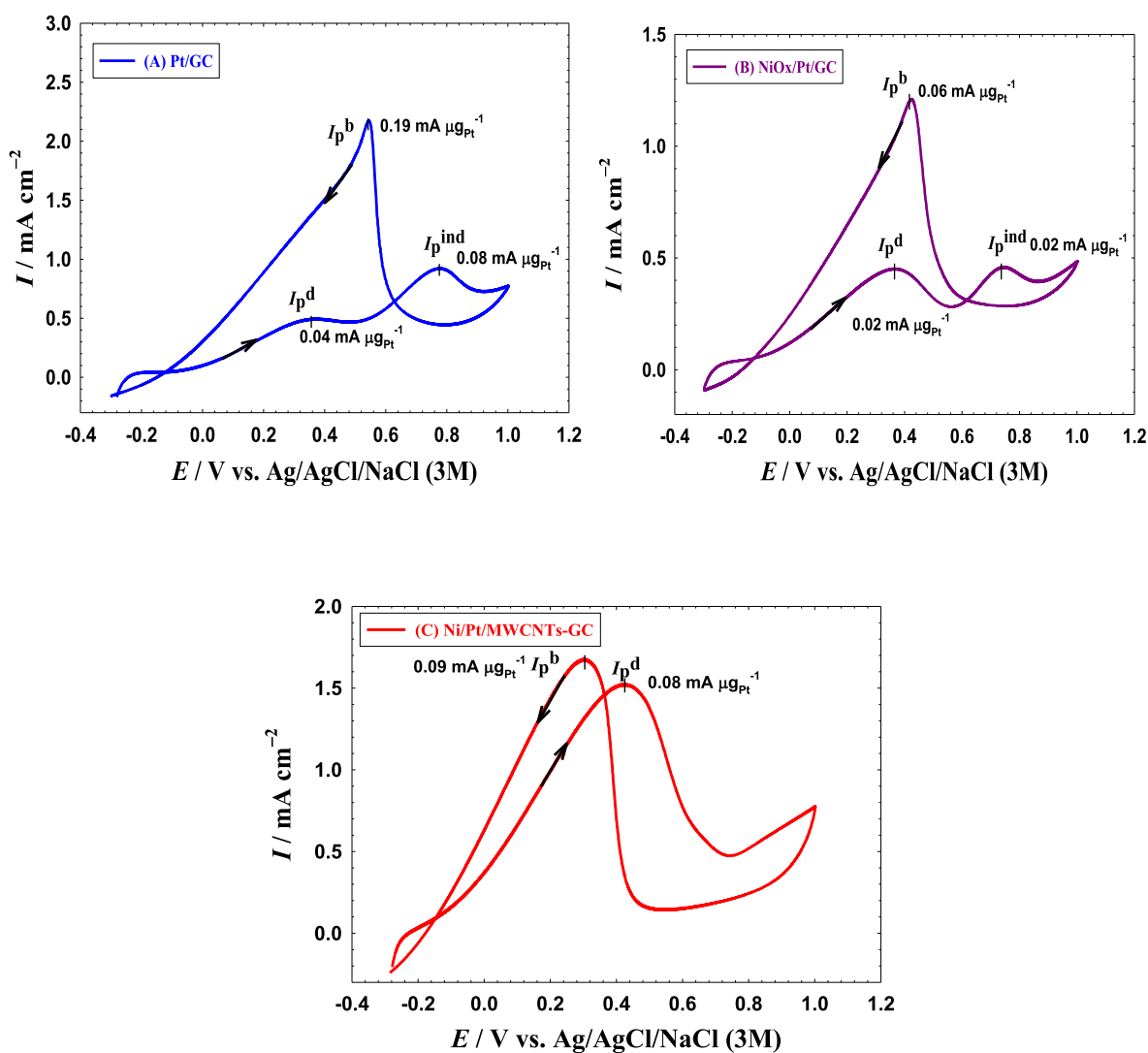


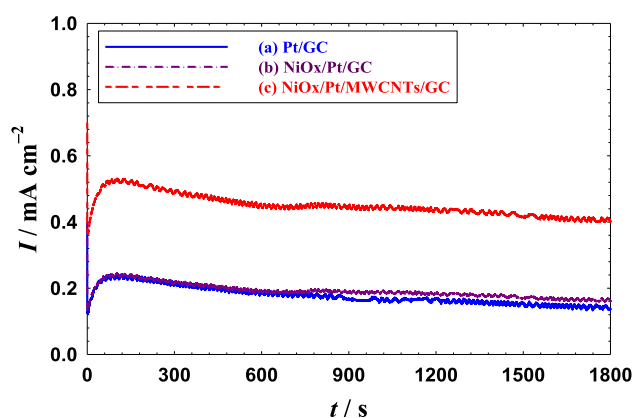
Fig. 6 CVs obtained at the (a) Pt/GC, (b) NiOx/Pt/GC and (c) NiOx/Pt/CNTs/GC electrodes in 0.3 M FA (pH = 3.5). Potential scan rate: 100 mVs^{-1} .

Table 3 Indices of the electrochemical activities of the catalysts (data were extracted from Fig. 6).

Electrode	I_p^d/I_p^{ind}	I_p^d/I_p^b	E_{onset} (V)
Pt/GC	0.69	0.17	-0.026
NiOx/Pt/GC	3.33	0.40	-0.028
NiOx/Pt/CNTs/GC	∞	0.93	-0.142

Table 4 A comparison of the electrocatalytic activities of several catalysts toward EOFa.

Electrode	I_p^d/I_p^{ind}	Reference
Pt/GC	0.69	This investigation
NiOx/Pt/GC	3.33	This investigation
NiOx/Pt/CNTs/GC	∞	This investigation
Commercial Pt/C	0.16	(Pei et al., 2020)
Pt _{11.1} Ni _{88.9} /C	0.33	(Pei et al., 2020)
Pt _{10.9} Au _{0.2} Ni _{88.9} /C	0.34	(Pei et al., 2020)
Pt/C	0.29	(Çögenli and Yurtcan, 2018)
Pt black	0.24	(Çögenli and Yurtcan, 2018)
PtPd/C	0.87	(Çögenli and Yurtcan, 2018)
Pt/PDAN/GC	0.72	(Shatla et al., 2019)
Pd/Pt/PDAN/GC	1.2	(Shatla et al., 2019)
Pt/Pd/PDAN/GC	1.7	(Shatla et al., 2019)
Pt-TiOx (700 °C)	10	(Al-Akraa and Mohammad, 2020)
Pt/MWCNTs-GC	7.5	(Al-Akraa et al., 2019a)
MnOx/Au/Pt/GC	30.2	(Mohammad et al., 2018)
NiOx/Au/Pt/GC	∞	(Mohammad et al., 2015)
Au/Pt/GC	3.44	(Al-Akraa et al., 2019c)
Au ₂₃ /Pt ₆₃ Co ₁₄	3.6	(Sun et al., 2021)
NP-PtAu ₂	0.79	(Wen et al., 2021)

**Fig. 7** Current transients obtained at the (a) Pt/GC, (b) NiOx/Pt/GC and (c) NiOx/Pt/CNTs/GC electrodes in 0.3 M FA (pH = 3.5) at 0.20 V.

3.4. Mechanisms of enhancement

The electrochemical impedance spectroscopy (EIS) technique was utilized to assess the charge transfer resistance (R_{ct}) of the proposed modified catalysts during EOFa. Fig. 8 shows the Nyquist plots obtained at the Pt/GC, NiOx/Pt/GC and

NiOx/Pt/CNTs/GC electrodes in a 0.3 M aqueous solution of FA (pH = 3.5) at a potential of 0.2 V in the frequency range (10 mHz to 100 kHz). The fitting was carried out by the EC-Lab software and the equivalent circuit of this system was displayed in the inset of Fig. 8. Over there, the R_{ct} , R_s and C_{dl} referred to the charge transfer resistance associating EOFa, solution resistance and double layer capacitance, respectively. Principally, R_{ct} that is equivalent to the polarization resistance of the electrochemical system is defined by the diameter of the extrapolated semicircle in the Nyquist diagram (RIBEIRO et al., 2015). In this regard, the larger the semicircle diameter, the higher R_{ct} , and consequently, the slower kinetics of the reaction (Yavuz et al., 2015). Fig. 8 depicts lower R_{ct} (0.58 and 0.62 k Ω), respectively, at the NiOx/Pt/GC and NiOx/Pt/CNTs/GC electrodes compared to 3.04 k Ω obtained at the Pt/GC electrode (data are summarized in Table 6). In fact, the difference between R_{ct} of the NiOx/Pt/GC catalyst (0.58 k Ω) and that of the NiOx/Pt/CNTs/GC catalyst (0.62 k Ω) was not large and it might result from a geometrical change in the preferred orientation of n-NiOx for EOFa. We indicated that CNTs had almost no electronic role in the catalytic enhancement in the EOFa, in contrast to n-NiOx which owned, exclusively, the electronic influence. Nevertheless, the addition of CNTs to the catalyst seemed to encounter a little the electronic influence of n-NiOx. This will be confirmed later (see Fig. 10) as the peak voltage of the CO desorption was shifted back to a more positive potential after the amendment of the NiOx/Pt/GC catalyst with CNTs. The ICP analysis (Table 5) also indicated a faster rate for the dissolution of Ni in the NiOx/Pt/CNTs/GC electrode than that of the NiOx/Pt/GC electrode which could also affect R_{ct} . The lower values of R_{ct} of the NiOx/Pt/GC and NiOx/Pt/CNTs/GC electrodes inferred the facilitated charge transfer and boosted catalytic activity of them toward EOFa. Nonetheless, the origin of enhancement at the NiOx/Pt/CNTs/GC electrode might not be only electronic as this catalyst was much better than the NiOx/Pt/GC catalyst toward EOFa (Fig. 6). An extra geometrical effect might influence the catalytic activity of the NiOx/Pt/CNTs/GC catalyst.

To further investigate the kinetics of EOFa, Tafel measurements were conducted under a steady-state condition (Gharib and Arab, 2021). As shown in Fig. 9, the Tafel slopes (b) for the NiOx/Pt/GC (91 mV/decade, Fig. 9b) and NiOx/Pt/CNTs/GC (89 mV/decade, Fig. 9c) electrodes showed a much lower value than that of Pt/GC (120 mV/decade, Fig. 9a). As known, the Tafel slope is inversely proportional to $(1 - \alpha)$ where α denotes the transfer coefficient and $(1 - \alpha)$ assesses the contribution of the electrical component in lowering the activation energy or speeding the kinetics of EOFa. Lowering the Tafel slope corresponded to an increase of $(1 - \alpha)$ which necessitated a reduction in the activation energy and boosting the kinetics of EOFa. This can likely originate with a higher CO tolerance (Zhang et al., 2013). Table 6 provided a summary of the Tafel slopes obtained from Fig. 9. So far, the Nyquist and Tafel plots of the NiOx/Pt/GC and NiOx/Pt/CNTs/GC electrodes explored the responsibility of n-NiOx to the electronic enhancement but the role of CNTs was still unclear.

To precisely recognize the effect of CNTs, CO was allowed to chemisorb from 0.5 M FA at open-circuit potentials onto the Pt/GC, NiOx/Pt/GC and NiOx/Pt/CNTs/GC electrodes for 10 min before stripping in 0.5 M Na₂SO₄ (pH = 3.5) as

Table 5 ICP-OES data for the inspected catalysts after the electrochemical measurements.

Analyte	Wavelength/ nm	Electrode	Conc (sample)/ mgL ⁻¹	Detection limit/ mgL ⁻¹
Pt	214.424	Pt/GC	N.D*	1
		NiOx/Pt/GC	N.D*	
		NiOx/Pt/CNTs/GC	N.D*	
Ni	231.604	NiOx/Pt/GC	0.56	0.1
		NiOx/Pt/CNTs/GC	0.66	

* N.D: Not detectable.

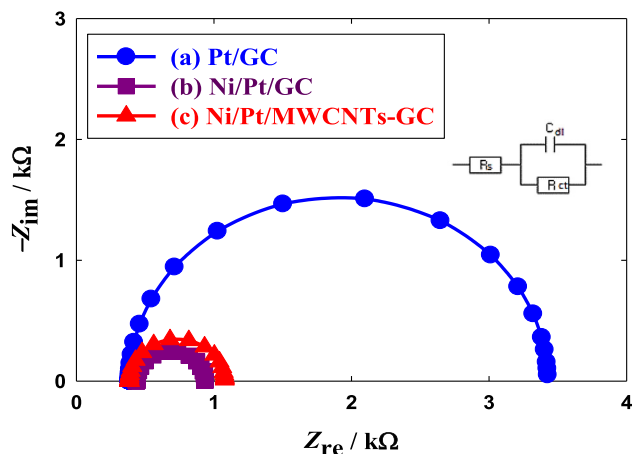


Fig. 8 Nyquist plot recorded at AC potential amplitude of 0.20 V obtained at the (a) Pt/GC, (b) NiOx/Pt/GC and (c) NiOx/Pt/CNTs/GC electrodes in 0.3 M FA (pH = 3.5). Frequency range from 10 mHz to 100 kHz. The fitting has been carried out by the EC-Lab software and the equivalent circuit of this system was displayed in the inset.

shown in Fig. 10. At the Pt/GC electrode (Fig. 10a), CO was oxidized at a potential (E_{CO}) of ca. 0.70 V with a peak charge (Q_{CO} , that is related to the amount of adsorbed CO) of ca. 1.08 mC. On the NiOx/Pt/GC electrode, CO oxidation started earlier with a negative shift of ca. 0.04 V in the E_{CO} along with a further decrease of ca. 0.13 mC in the Q_{CO} (see Fig. 10b). This again highlighted the effectiveness of the modification with n-NiOx in improving the electronic properties of the Pt surface that weakened the Pt-CO bonding and facilitated the oxidative removal of poisoning CO (Mohammad et al., 2015).

Interestingly, at the NiOx/Pt/CNTs/GC electrode (Fig. 10c), the E_{CO} was midway between those of the Pt/GC and NiOx/Pt/GC catalysts but much closer to that of the Pt/GC catalyst, but the least amount (ca. 0.44 mC) of adsorbed CO was observed for this catalyst. Table 6 summarizes the E_{CO} and Q_{CO} values obtained from Fig. 10. It seemed that CNTs participated geometrically in the catalytic enhancement

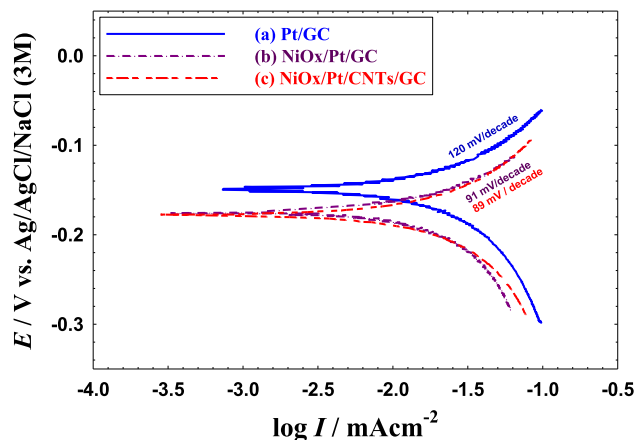


Fig. 9 Quasi-steady-state polarization curves for the EOFA obtained at the (a) Pt/GC, (b) NiOx/Pt/GC and (c) NiOx/Pt/CNTs/GC electrodes in 0.3 M FA (pH = 3.5). Potential scan rate: 100 mVs⁻¹.

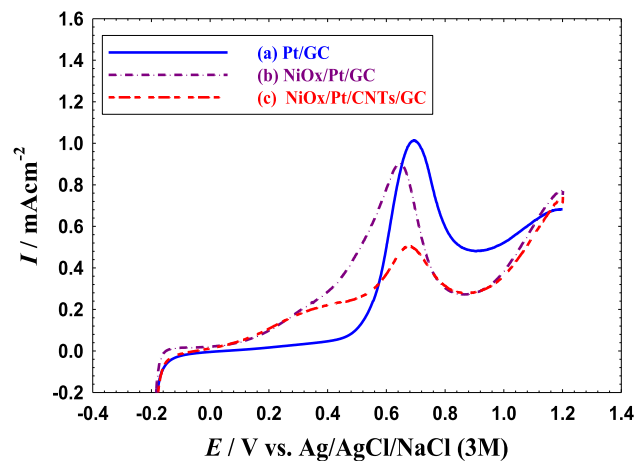


Fig. 10 LSVs for oxidative CO stripping obtained at the (a) Pt/GC, (b) NiOx/Pt/GC and (c) NiOx/Pt/CNTs/GC electrodes in 0.5 M Na₂SO₄ (pH = 3.5). Potential scan rate: 50 mVs⁻¹. Before measurements, CO was adsorbed from 0.5 M FA at the open circuit potential for 10 min.

Table 6 Summary of the electrochemical data extracted from Figs. 8, 9 and 10.

Electrode	R_{ct} (kΩ)	b (mVdecade ⁻¹)	E_{CO} (V)	Q_{CO} (mC)
Pt/GC	3.04	120	0.70	1.08
NiOx/Pt/GC	0.58	91	0.64	0.95
NiOx/Pt/CNTs/GC	0.62	89	0.68	0.44

of EOFA (Al-Akraa et al., 2019a; Al-Akraa et al., 2019b). As reported previously, CNTs could facilitate the deposition of well-dispersed n-Pt that assisted in decreasing the possibility of CO adsorption at the Pt surface. This was beside its high electronic conductivity, high corrosion resistance, and good structural, mechanical and chemical stability (Ren et al., 2020). To sum up, the NiOx/Pt/CNTs/GC electrode acquired not only an electronic but also a geometric enhancement toward EOFA by the modification of the Pt/GC electrode with n-NiOx and CNTs, respectively.

4. Conclusion

A propitious CNTs-amended NiOx/Pt catalyst was fabricated for efficient EOFA. The electrocatalytic performance of the NiOx/Pt/CNTs/GC catalyst was compared with those of the Pt/GC and NiOx/Pt/GC catalysts. The NiOx/Pt/CNTs/GC electrode retained the highest catalytic performance toward EOFA where it mitigated completely the undesirable CO poisoning and sustained up to five times (compared to the behavior of the Pt/GC catalyst) increase in the reaction reversibility and poisoning tolerance. The role of n-NiOx in the catalytic enhancement was proved to be principally electronic; in contrast to CNTs that influenced the reaction kinetics geometrically. The long-lasting durability of the NiOx/Pt/CNTs/GC catalyst predicted a bright future for the DFAFCs.

Declaration of Competing Interest

The authors declare that they have no known competing financial interests or personal relationships that could have appeared to influence the work reported in this paper.

References

- Abd El-Moghny, M.G., Alalawy, H.H., Mohammad, A.M., Mazhar, A.A., El-Deab, M.S., El-Anadouli, B.E., 2017. Conducting polymers inducing catalysis: Enhanced formic acid electro-oxidation at a Pt/polyaniline nanocatalyst. *Int. J. Hydrog. Energy* 42, 11166–11176.
- Al-Akraa, I.M., Asal, Y.M., Darwish, S.A., 2019a. A simple and effective way to overcome carbon monoxide poisoning of platinum surfaces in direct formic acid fuel cells. *Int. J. Electrochem. Sci.* 14, 8267–8275.
- Al-Akraa, I.M., Asal, Y.M., Khalifa, A.A., 2019b. A promising modification of Pt surfaces with CNTs for decreasing poisoning impact in direct methanol fuel cells. *Int. J. Electrochem. Sci.* 14, 8276–8283.
- Al-Akraa, I.M., Asal, Y.M., Mohammad, A.M., 2019c. Facile synthesis of a tailored-designed Au/Pt nanoanode for enhanced formic acid, methanol, and ethylene glycol electrooxidation. *J. Nanomater.* 2019, 2784708.
- Al-Akraa, I.M., Mohammad, A.M., 2020. A spin-coated TiOx/Pt nanolayered anodic catalyst for the direct formic acid fuel cells. *Arab. J. Chem.* 13, 4703–4711.
- Al-Akraa, I.M., Mohammad, A.M., El-Deab, M.S., El-Anadouli, B. E., 2015a. Electrocatalysis by design: Synergistic catalytic enhancement of formic acid electro-oxidation at core-shell Pd/Pt nanocatalysts. *Int. J. Hydrog. Energy* 40, 1789–1794.
- Al-Akraa, I.M., Mohammad, A.M., El-Deab, M.S., El-Anadouli, B.E., 2017. Flower-shaped gold nanoparticles: preparation, characterization, and electrocatalytic application. *Arab. J. Chem.* 10, 877–884.
- Al-Akraa, I.M., Mohammad, A.M., El-Deab, M.S., El-Anadouli, B. E., 2018. Fabrication of CuOx-Pd nanocatalyst supported on a glassy carbon electrode for enhanced formic acid electro-oxidation. *J. Nanotechnol.* 2018, 3803969.
- Al-Akraa, I.M., Mohammad, A.M., El-Deab, M.S., El-Anadouli, B. S., 2015b. Advances in direct formic acid fuel cells: fabrication of efficient Ir/Pd nanocatalysts for formic acid electro-oxidation. *Int. J. Electrochem. Sci.* 10, 3282–3290.
- Al-Akraa, I.M., Ohsaka, T., Mohammad, A.M., 2019d. A promising amendment for water splitters: Boosted oxygen evolution at a platinum, titanium oxide and manganese oxide hybrid catalyst. *Arab. J. Chem.* 12, 897–907.
- Al-Qodami, B.A., Farrag, H.H., Sayed, S.Y., Allam, N.K., El-Anadouli, B.E., Mohammad, A.M., 2018. Bifunctional tailoring of platinum surfaces with earth abundant iron oxide nanowires for boosted formic acid electro-oxidation. *J. Nanotechnol.* 2018, 4657040.
- Armenta-González, A.J., Carrera-Cerritos, R., Moreno-Zuria, A., Álvarez-Contreras, L., Ledesma-García, J., Cuevas-Muñiz, F.M., Arriaga, L.G., 2016. An improved ethanol microfluidic fuel cell based on a PdAg/MWCNT catalyst synthesized by the reverse micelles method. *Fuel* 167, 240–247.
- Asal, Y.M., Al-Akraa, I.M., Mohammad, A.M., El-Deab, M.S., 2019a. A competent simultaneously co-electrodeposited Pt-MnOx nanocatalyst for enhanced formic acid electro-oxidation. *J. Taiwan Inst. Chem. Eng.* 96, 169–175.
- Asal, Y.M., Al-Akraa, I.M., Mohammad, A.M., El-Deab, M.S., 2019b. Design of efficient bimetallic Pt–Au nanoparticle-based anodes for direct formic acid fuel cells. *Int. J. Hydrog. Energy* 44, 3615–3624.
- Asazawa, K., Yamada, K., Tanaka, H., Taniguchi, M., Oguro, K., 2009. Electrochemical oxidation of hydrazine and its derivatives on the surface of metal electrodes in alkaline media. *J. Power Sources* 191, 362–365.
- Cabañas Polo, S., Ferrari, B., Gordo, E., Sánchez-Herencia, A., Argirusis, C., 2012. Nanosized nickel powders synthesized by a reduction method assisted by ultrasound. *Proceedings of the International Euro Powder Metallurgy Congress and Exhibition.*
- Chen, J.H., Li, W.Z., Wang, D.Z., Yang, S.X., Wen, J.G., Ren, Z.F., 2002. Electrochemical characterization of carbon nanotubes as electrode in electrochemical double-layer capacitors. *Carbon* 40, 1193–1197.
- Çögenli, M.S., Yurtcan, A.B., 2018. Catalytic activity, stability and impedance behavior of PtRu/C, PtPd/C and PtSn/C bimetallic catalysts toward methanol and formic acid oxidation. *Int. J. Hydrog. Energy* 43, 10698–10709.
- Cruz-Reyes, I., Trujillo-Navarrete, B., García-Tapia, K., Salazar-Gastélum, M.I., Paraguay-Delgado, F., Félix-Navarro, R.M., 2020. Pd/MnO₂ as a bifunctional electrocatalyst for potential application in alkaline fuel cells. *Fuel* 279, 118470.
- El-Deab, M.S., El-Nowihy, G.H., Mohammad, A.M., 2015. Synergistic enhancement of the electro-oxidation of methanol at tailor-designed nanoparticle-based CoOx/MnOx/Pt ternary catalysts. *Electrochim. Acta* 165, 402–409.
- El-Nagar, G.A., El-Deab, M.S., Mohammad, A.M., El-Anadouli, B. E., 2015. Promoting effect of hydrocarbon impurities on the electro-oxidation of formic acid at Pt nanoparticles modified GC electrodes. *Electrochim. Acta* 180, 268–279.
- El-Nagar, G.A., Mohammad, A.M., El-Deab, M.S., El-Anadouli, B. E., 2013. Electrocatalysis by design: Enhanced electrooxidation of formic acid at platinum nanoparticles–nickel oxide nanoparticles binary catalysts. *Electrochim. Acta* 94, 62–71.
- El-Nagar, G.A., Mohammad, A.M., El-Deab, M.S., El-Anadouli, B. E., 2017. Propitious dendritic Cu₂O–Pt nanostructured anodes for direct formic acid fuel cells. *ACS Appl. Mater. Interfaces* 9, 19766–19772.

- El Sawy, E.N., Pickup, P.G., 2019. Carbon monoxide and formic acid oxidation at Rh@ Pt nanoparticles. *Electrochim. Acta* 302, 234–240.
- Fazlali, F., Mahjoub, A., Abazari, R., 2015. A new route for synthesis of spherical NiO nanoparticles via emulsion nano-reactors with enhanced photocatalytic activity. *Solid State Sci.* 48, 263–269.
- Garg, A., Panda, B.N., Lam, J.S.L., 2016. Functional characterization of current characteristic of direct methanol fuel cell. *Fuel* 183, 432–440.
- Gharib, A., Arab, A., 2021. Improved formic acid oxidation using electrodeposited Pd–Cd electrocatalysts in sulfuric acid solution. *Int. J. Hydrog. Energy* 46, 3865–3875.
- Grey, C.P., Hall, D.S., 2020. Prospects for lithium-ion batteries and beyond—a 2030 vision. *Nat. Commun.* 11, 6279.
- Habibi, B., Delnavaz, N., 2011. Carbon–ceramic supported bimetallic Pt–Ni nanoparticles as an electrocatalyst for oxidation of formic acid. *Int. J. Hydrog. Energy* 36, 9581–9590.
- Hailong, Y., Deyang, Z., Xu, J., Lu, Y., Liu, Y., Qiu, K., Zhang, Y., Luo, Y., 2014. Solution growth of NiO nanosheets supported on Ni foam as high-performance electrodes for supercapacitors. *Nanoscale Res. Lett.* 9, 424.
- Huang, X., Li, F., Zhou, Q., Wu, G., Huang, Y., Wang, L., Liu, B., Cui, T., 2015. In situ synchrotron X-ray diffraction with laser-heated diamond anvil cells study of Pt up to 95 GPa and 3150 K. *RSC Adv.* 5, 14603–14609.
- Juodkazytė, J., Šebeka, B., Savickaja, I., Petrulėvičienė, M., Butkutė, S., Jasulaitienė, V., Selskis, A., Ramanauskas, R., 2019. Electrolytic splitting of saline water: Durable nickel oxide anode for selective oxygen evolution. *Int. J. Hydrog. Energy* 44, 5929–5939.
- Keller, T.M., Qadri, S.B., Little, C.A., 2004. Carbon nanotube formation in situ during carbonization in shaped bulk solid cobalt nanoparticle compositions. *J. Mater. Chem.* 14, 3063–3070.
- Kiani, M., Zhang, J., Luo, Y., Chen, Y., Chen, J., Fan, J., Wang, G., Wang, R., 2019. Facile synthesis and enhanced catalytic activity of electrochemically dealloyed platinum–nickel nanoparticles towards formic acid electro-oxidation. *J. Energy Chem.* 35, 9–16.
- Kim, S., Chen, J., Cheng, T., Gindulyte, A., He, J., He, S., Li, Q., Shoemaker, B.A., Thiessen, P.A., Yu, B., 2019. PubChem 2019 update: improved access to chemical data. *Nucleic Acids Res.* 47, D1102–D1109.
- Larsen, R., Ha, S., Zakzeski, J., Masel, R.I., 2006. Unusually active palladium-based catalysts for the electrooxidation of formic acid. *J. Power Sources* 157, 78–84.
- Li, S.-J., Guo, W., Yuan, B.-Q., Zhang, D.-J., Feng, Z.-Q., Du, J.-M., 2017. Assembly of ultrathin NiOOH nanosheets on electrochemically pretreated glassy carbon electrode for electrocatalytic oxidation of glucose and methanol. *Sens. Actuat. B: Chem.* 240, 398–407.
- Li, Z., Chen, Y., Ji, S., Tang, Y., Chen, W., Li, A., Zhao, J., Xiong, Y., Wu, Y., Gong, Y., Yao, T., Liu, W., Zheng, L., Dong, J., Wang, Y., Zhuang, Z., Xing, W., He, C.T., Peng, C., Cheong, W.C., Li, Q., Zhang, M., Chen, Z., Fu, N., Gao, X., Zhu, W., Wan, J., Zhang, J., Gu, L., Wei, S., Hu, P., Luo, J., Li, J., Chen, C., Peng, Q., Duan, X., Huang, Y., Chen, X.M., Wang, D., Li, Y., 2020. Iridium single-atom catalyst on nitrogen-doped carbon for formic acid oxidation synthesized using a general host-guest strategy. *Nat. Chem.* 12, 764–772.
- Li, Z., Song, M., Zhu, W., Zhuang, W., Du, X., Tian, L., 2021. MOF-derived hollow heterostructures for advanced electrocatalysis. *Coord. Chem. Rev.* 439, 213946.
- Lović, J.D., Tripković, A.V., Gojković, S.L.J., Popović, K.D., Tripković, D.V., Olszewski, P., Kowal, A., 2005. Kinetic study of formic acid oxidation on carbon-supported platinum electrocatalyst. *J. Electroanal. Chem.* 581, 294–302.
- Lu, L., Shen, L., Shi, Y., Chen, T., Jiang, G., Ge, C., Tang, Y., Chen, Y., Lu, T., 2012. New insights into enhanced electrocatalytic performance of carbon supported Pd–Cu catalyst for formic acid oxidation. *Electrochim. Acta* 85, 187–194.
- Mari, E., Tsai, P.-C., Eswaran, M., Ponnusamy, V.K., 2020. Efficient electro-catalytic oxidation of ethylene glycol using flower-like graphitic carbon nitride/iron oxide/palladium nanocomposite for fuel cell application. *Fuel* 280, 118646.
- Maturost, S., Pongpichayakul, N., Waenkaew, P., Promsawan, N., Themsirimongkon, S., Jakmunee, J., Saipanya, S., 2021. Electro-catalytic activity of bimetallic PtPd on cerium oxide-modified carbon nanotube for oxidation of alcohol and formic acid. *J. Electroanal. Chem.* 895, 115445.
- Maya-Cornejo, J., Guerra-Balcázar, M., Arjona, N., Álvarez-Contreras, L., Rodríguez Valadez, F.J., Gurrola, M.P., Ledesma-García, J., Arriaga, L.G., 2016. Electrooxidation of crude glycerol as waste from biodiesel in a nanofluidic fuel cell using Cu@Pt/C and Cu@Pt/C. *Fuel* 183, 195–205.
- Mohammad, A.M., Al-Akraa, I.M., El-Deab, M.S., 2018. Superior electrocatalysis of formic acid electro-oxidation on a platinum, gold and manganese oxide nanoparticle-based ternary catalyst. *Int. J. Hydrog. Energy* 43, 139–149.
- Mohammad, A.M., El-Nagar, G.A., Al-Akraa, I.M., El-Deab, M.S., El-Anadoul, B.E., 2015. Towards improving the catalytic activity and stability of platinum-based anodes in direct formic acid fuel cells. *Int. J. Hydrog. Energy* 40, 7808–7816.
- Ong, A.L., Inglis, K.K., Whelligan, D.K., Murphy, S., Varcoe, J.R., 2015. Effect of cationic molecules on the oxygen reduction reaction on fuel cell grade Pt/C (20 wt%) catalyst in potassium hydroxide (aq, 1 mol dm⁻³). *Phys. Chem. Chem. Phys.* 17, 12135–12145.
- Ong, B.C., Kamarudin, S.K., Basri, S., 2017. Direct liquid fuel cells: a review. *Int. J. Hydrog. Energy* 42, 10142–10157.
- Pei, A., Ruan, L., Liu, B., Chen, W., Lin, S., Chen, B., Liu, Y., Zhu, L. H., Chen, B.H., 2020. Ultra-low Au decorated PtNi alloy nanoparticles on carbon for high-efficiency electro-oxidation of methanol and formic acid. *Int. J. Hydrog. Energy* 45, 22893–22905.
- Ren, J., Zhang, J., Yang, C., Yang, Y., Zhang, Y., Yang, F., Ma, R., Yang, L., He, H., Huang, H., 2020. Pd nanocrystals anchored on 3D hybrid architectures constructed from nitrogen-doped graphene and low-defect carbon nanotube as high-performance multifunctional electrocatalysts for formic acid and methanol oxidation. *Mater. Today Energy* 16, 100409.
- Ribeiro, D.V., Souza, C.A.C., Abrantes, J.C.C., 2015. Use of Electrochemical Impedance Spectroscopy (EIS) to monitoring the corrosion of reinforced concrete. *Rev. IBRACON Estrut. Mater.* 8, 529–546.
- Shatla, A.S., Hassan, K.M., Abd-El-Latif, A.A., Hathoot, A.A., Baltruschat, H., Abdel-Azzem, M., 2019. Poly 1,5 diamionaphthalene supported Pt, Pd, Pt/Pd and Pd/Pt nanoparticles for direct formic acid oxidation. *J. Electroanal. Chem.* 833, 231–241.
- Shi, H., Liao, F., Zhu, W., Shao, C., Shao, M., 2020. Effective PtAu nanowire network catalysts with ultralow Pt content for formic acid oxidation and methanol oxidation. *Int. J. Hydrog. Energy* 45, 16071–16079.
- Sun, Y., Huang, B., Li, Y., Qin, Y., Fu, Z., Sun, M., Wang, L., Guo, S., 2021. Segmented Au/PtCo heterojunction nanowires for efficient formic acid oxidation catalysis. *Fun. Res.*, <https://doi.org/10.1016/j.fmre.2021.06.016>.
- Tanveer, M., Su Lim, E., Kim, K.-Y., 2021. Effects of channel geometry and electrode architecture on reactant transportation in membraneless microfluidic fuel cells: a review. *Fuel* 298, 120818.
- Wen, X., Yin, S., Yin, H., Ding, Y., 2021. A displacement dealloying route to dilute nanoporous PtAu alloys for highly active formic acid electro-oxidation. *Electrochim. Acta* 373, 137884.
- Xie, Y., Dimitrov, N., 2020. Ultralow Pt loading nanoporous Au-Cu-Pt thin film as highly active and durable catalyst for formic acid oxidation. *Appl. Catal. B* 263, 118366.
- Xu, H., Shang, H., Wang, C., Du, Y., 2020a. Low-dimensional metallic nanomaterials for advanced electrocatalysis. *Adv. Funct. Mater.* 30, 2006317.
- Xu, H., Shang, H., Wang, C., Du, Y., 2020b. Ultrafine Pt-based nanowires for advanced catalysis. *Adv. Funct. Mater.* 30, 2000793.

- Yavuz, E., Özdokur, K.V., Çakar, İ., Koçak, S., Ertaş, F.N., 2015. Electrochemical preparation, characterization of molybdenum-oxide/platinum binary catalysts and its application to oxygen reduction reaction in weakly acidic medium. *Electrochim. Acta* 151, 72–80.
- Yoo, J.K., Rhee, C.K., 2016. Formic acid oxidation on Bi-modified Pt surfaces: Pt deposits on Au versus bulk Pt. *Electrochim. Acta* 216, 16–23.
- Yu, Z.-Y., Huang, R., Liu, J., Luo, C.-X., Wang, C.-Y., Song, Q.-T., Xiao, C., Yin, S.-H., Xu, B.-B., Sun, S.-G., 2020. PdPt concave nanocubes directly electrodeposited on carbon paper as high active and durable catalysts for formic acid and ethanol oxidation. *Electrochim. Acta* 354, 136654.
- Zhang, Q., Yue, R., Jiang, F., Wang, H., Zhai, C., Yang, P., Du, Y., 2013. Au as an efficient promoter for electrocatalytic oxidation of formic acid and carbon monoxide: a comparison between Pt-on-Au and PtAu alloy catalysts. *Gold Bull.* 46, 175–184.
- Zhou, W., Xu, J., Du, Y., Yang, P., 2011. Polycarbazole as an efficient promoter for electrocatalytic oxidation of formic acid on Pt and Pt–Ru nanoparticles. *Int. J. Hydrog. Energy* 36, 1903–1912.